Sensitivity of the Equatorial Air–Sea Coupled System to the Zonal Phase Difference between SST and Wind Stress①

Soon-Il An

International Pacific Research Center, SOEST, University of Hawaii at Manoa, Honolulu, Hawaii 96822, USA

In-Sik Kang

School of Earth Environment Sciences, Seoul National University, Seoul, 151-742, Korea

(Received April 17, 2000, revised September 21, 2000)

ABSTRACT

An eigen analysis of the equatorial air–sea coupled model is carried out to understand the mechanism of the slowly varying mode for various zonal phase differences between SST and wind stress. The frequency and growth rate of the slow mode highly depend on the zonal phase difference between SST and wind stress anomalies and the wave scale. For ultra-long waves longer than 20,000 km, the system propagates westward regardless of the position of wind stress. However, for the long waves observed in the Pacific, the slow mode tends to propagate eastward when the SST and wind stress anomalies are close to each other (within a quadrature phase relationship). On the other hand, when the wind stress is located far away from SST, the slow mode tends to propagate westward. The coupled system produces the unstable modes when the westerly (easterly) wind stress is located in the west of warm (cold) SST. It is noted that for the Pacific basin scale, the eastward propagating unstable waves can be produced when the wind stress is located to the west of SST with a few thousand kilometer distance. Also examined in the present study is the relative role of the thermocline displacement and zonal advection effects in determining the propagation and instability of the coupled system.

Key words: Air–sea coupled system, El Niño, Slow mode

1. Introduction

Many studies using a variety of coupled models have reproduced ENSO like features (e.g., Hirst, 1986, 1988; Zebiak and Cane, 1987; Battisti and Hirst, 1989; Jin and Neelin, 1993; Jin, 1997; Kirtman, 1997; Kang and An, 1998; Wakata and Sarachik, 1991). But, a variety of solutions have been reported depending on different parameterizations of atmospheric processes, particularly the relationship between wind stress and SST anomaly, indicating that the relationship has a large impact on the air–sea coupled system in the tropical Pacific.

In some of those coupled models (Hirst, 1986; Battisti and Hirst, 1989; Wakata and Sarachik, 1991), atmospheric heating anomaly is assumed to be proportional to local SST anomaly. But in reality, the region of SST anomaly does not match that of anomalous atmospheric heating. Moreover, the same SST forcing produces different wind anomalies in the tropical Pacific according to the season and decades (An and Wang, 2000), because the atmospheric response depends not only on the local SST anomaly but also on the atmospheric and oceanic basic states (Horeling et al., 1997). It is also noted that the simulated wind

①Corresponding author address: Prof. In-Sik Kang, Department of Atmospheric Sciences, Seoul National University, Seoul, 151-742, Korea, kang@climate.snu.ac.kr

stresses with intermediate and fully coupled models are somewhat different from the observed ones (Perigaud and Dewitte, 1996). In particular, the wind stress anomalies simulated by the Cane and Zebiak's (1985) intermediate coupled model are shifted to the east about 30 degrees compared to the observations (Dewitte and Perigaud, 1996). Kang and Kug (2000) demonstrated that a better representation of wind stress improves the ENSO predictability of the Cane and Zebiak's model. Although many studies mentioned above indicate that the characteristics of air–sea coupled system and its predictability depend on the representation of wind stress in terms of SST anomalies, the impact of their relationship on the coupled system is not fully investigated yet.

In the present study, we investigated how the characteristics of air–sea coupled system, such as the frequency and growth rate and spatial pattern, are sensitive to the zonal phase relationship between wind and SST anomalies. Based on the results, we can access a range of the zonal phase shift (location) of wind stress with respect to SST anomalies in the equatorial Pacific. Section 2 shows the formulation of the present air–sea coupled model, which produces the slow mode. In Section 3, the analytic solution of this coupled model is obtained, and the results of the sensitivity test to the zonal phase difference between the SST and wind stress are discussed. In Section 4, the relative role of thermocline displacement and zonal advection effects in determining the propagation and instability of the coupled mode is examined. Summary is given in Section 5.

2. Model

In this study, we use a linear, reduced gravity wave equation for the coupled system. For simplification, we remove the meridional component of the atmospheric and oceanic variables, because the forced part of oceanic response to the zonal wind stress is dominated by the zonal component near the equator. The meridional component is also induced by the zonal forcing in a rotating system, but it is small near the equator because of a small Coriolis parameter. To consider this special condition at the equator, the present model is based on a non–rotating system and, as a result, the response to zonal forcing has a zonal component only. The present system is similar to that used by Lau (1981).

The zonal phase difference (θ) between SST and the wind stress anomalies is prescribed in the present study. The positive (negative) θ indicates that the wind stress is located to the east (west) of SST. The governing equations for the atmosphere and ocean, which have been nondimensionalized with respect to a length scale of $(C_o / \beta)^{1/2}$ and a time scale of $(C_o / \beta)^{-1/2}$ where C_o is the oceanic gravity speed and β the meridional derivative of the Coriolis parameter, can be written as follows:

ATMOSPHERE:

$$AU + \frac{\partial \Theta}{\partial x} = 0, \tag{1a}$$

$$B\Theta + C^2 \frac{\partial U}{\partial x} = -Q_a, \tag{1b}$$

where U is the anomalous zonal wind; Θ the pressure perturbation; A and B the Rayleigh friction and Newtonian cooling coefficients, respectively; C the ratio between the atmospheric and oceanic gravity wave speed, defined as C_a / C_o; Q_a the atmospheric heating parameterized as $K_Q T e^{-i\theta^*}$, where T is the SST anomaly. Thus, the atmospheric heating is

proportional to SST anomaly with a phase difference of θ^*. By combining Eqs. (1a) and (1b), the zonal phase difference (θ) between the wind stress and SST anomalies is easily identified as $\theta^* - \pi/2$.

OCEAN:

$$\frac{\partial u}{\partial t} + \frac{\partial h}{\partial x} = \tau - au, \tag{2a}$$

$$\frac{\partial h}{\partial t} + \frac{\partial u}{\partial x} = -ah, \tag{2b}$$

$$\frac{\partial T}{\partial t} = -\lambda u + \sigma h - bT, \tag{2c}$$

where u is the zonal current anomaly; h the upper-layer thickness perturbation (equally thermocline depth anomaly); τ the zonal wind stress anomaly parameterized as γU; a and b the coefficients of Rayleigh friction and Newtonian cooling, respectively; λ and σ the zonal gradient of mean SST and the entrainment thermal forcing coefficient, respectively. The coefficients used in this model are summarized in Table 1.

Table 1. Basic parameters and their values used in the present model

Parameters	Symbol and values
Atmospheric Rayleigh friction	$A = 5.8 \times 10^{-6}\,s^{-1}$
Atmospheric Newtonian cooling rate	$B = 5.8 \times 10^{-6}\,s^{-1}$
Oceanic Rayleigh friction	$a = 1.3 \times 10^{-8}\,s^{-1}$
Oceanic Newtonian cooling rate	$b = 9.3 \times 10^{-8}\,s^{-1}$
Atmospheric gravity wave speed	$C_a = 60.0\ m\ s^{-1}$
Oceanic gravity wave speed	$C_o = 2.9\ ms^{-1}$
Wind stress coupling coefficient	$\gamma = 1.6 \times 10^{-7}\,s^{-1}$
Background zonal SST gradient	$\lambda = 5.0 \times 10^{-7}\,K\ m^{-1}$
Entrainment thermal forcing coefficient	$\sigma = 5.0 \times 10^{-9}\,K\ m^{-1}s^{-1}$
SST-evaporation coefficient	$K_Q = 7.0 \times 10^{-3}\,m^2s^{-3}K^{-1}$
Mean upper layer depth	$H = 150m$
Reduced gravity	$G' = 0.056\ m\ s^{-1}$

3. Eigenmodes of the coupled system for different θ

After applying a sinusoidal wave solution to Eqs. (1) and (2) in the longitude and time, we can derive a dispersion relationship that is a cubic equation of frequency (ω). The three roots are a slow mode with low frequency, and eastward- and westward-propagating modes with high frequency. By neglecting the second- and third-order terms in the ω equation under the low-frequency limit, one can take out high-frequency modes in the coupled system. Then, we have a dispersion relationship associated with the slow mode. This mode has been a good prototype for slowly propagating coupled modes in various models (e.g., Anderson and McCreary, 1985; Meehl, 1990; Lau et al., 1992). The frequency (ω_R) and the growth rate (ω_I) of this slow mode are

$$\omega_R = \frac{X_1 Y_3 \cos\theta + (X_1 Y_2 - X_2 Y_1)\sin\theta - Y_1 Y_3}{X_1^2 + Y_1^2 - 2X_1 Y_1 \cos\theta} \tag{3a}$$

$$\omega_I = \frac{(X_1 Y_2 + X_2 Y_1)\cos\theta - X_1 Y_3 \sin\theta - X_1 X_2 - Y_1 Y_2}{X_1^2 + Y_1^2 - 2X_1 Y_1 \cos\theta} \tag{3b}$$

where

$$X_1 = (k^2 + a^2 + 2ab)(AB + k^2 C^2), \quad X_2 = b(k^2 + a^2)(AB + k^2 C^2),$$
$$Y_1 = kK_Q \gamma\lambda, \quad Y_2 = akK_Q \gamma\lambda, \quad Y_3 = k^2 K_Q \gamma\sigma,$$

X_1 and X_2 are related to the damping processes; Y_1 and Y_2 are related to the zonal advection as shown in the first term of Eq. (2c), and Y_3 is related to the vertical advection due to the change of thermocline depth anomaly as indicated in the second term of Eq. (2c); and k is the zonal wave number.

In order to show the sensitivity of the eigenmode to θ, we calculate the growth rate and frequency in the $k-\theta$ plan using the dispersion equation (3). As shown in Fig. 1, all major characteristics of the eigenmode such as instability, frequency, and propagating direction are highly dependent on θ. The unstable regimes appear for the large scale waves ($0.04 < k < 0.2$) and the negative θ ($-150^\circ < \theta < 0^\circ$). Again, the negative θ indicates the wind stress anomaly located to the west of SST anomaly. In Fig. 1b, the positive (negative) frequency indicates the eastward (westward) propagation. The coupled mode propagates to the east for $|\theta| < 80^\circ$ and $k > 0.1$ and to the west for $|\theta| > 80^\circ$ and $k > 0.1$. In the extremely large scale regime for $k < 0.1$, the coupled mode always propagates westward. It is noted that for a Pacific spatial scale $k = 0.15$ (wavelength = 15,000 km), the coupled system has an unstable eastward propagating mode when the wind stress is located to the west with a phase difference in a range of $-84^\circ < \theta < -30^\circ$. This indicates that an unstable coupled mode can be generated only when the wind stress is located to the west of SST with few thousand kilometer distance.

The spatial distributions of SST, thermocline depth, zonal current and wind stress anomalies of the eigenvector for $k = 0.15$ and $\theta = -72^\circ$ are shown in Fig. 2. The value of θ is chosen because the coupled mode is most unstable for the spatial scale of $k = 0.15$. The growth rate and period of the mode are 0.26 yr^{-1} and 6.2 years, respectively. The corresponding phase speed is 7.7 cm s^{-1}. The zonal phase relationship among those variables is calculated by using the equations of the eigenvector shown in the appendix. Figure 2 shows that the unstable mode with the wind stress anomaly located at 72° west of the SST has the thermocline depth anomaly shifted 18° to the east of SST, the zonal current located 45° to the west of SST, and the thermocline depth and wind stress in a quadrature relationship. This quadrature relationship results from the balance between the wind stress and the zonal gradient of thermocline depth. This balance is a very good approximation in the equatorial Pacific (Jin, 1997).

The spatial structure of the unstable ocean–atmosphere coupled mode shown in Fig. 2 is schematically illustrated in Fig. 3a. In this case, both the zonal SST advection (the second term in Eq. (2c)) and the vertical advection by the thermocline change (the third term in Eq. (2c), hereafter referred to as "thermocline effect") produce warming in the warm SST region. Such a net warming in the warm SST region results in the instability. It is noted that the thermocline effect is larger than the zonal advection effect in the present system. Thus, the system moves to the east because the maximum thermocline effect is located to the east of SST. Fig. 3b, on the other hand, shows the eastward propagating damping mode resulted from a slight shift (e.g., $\theta = 15^\circ$) of the wind stress to the east of SST. The figure is also

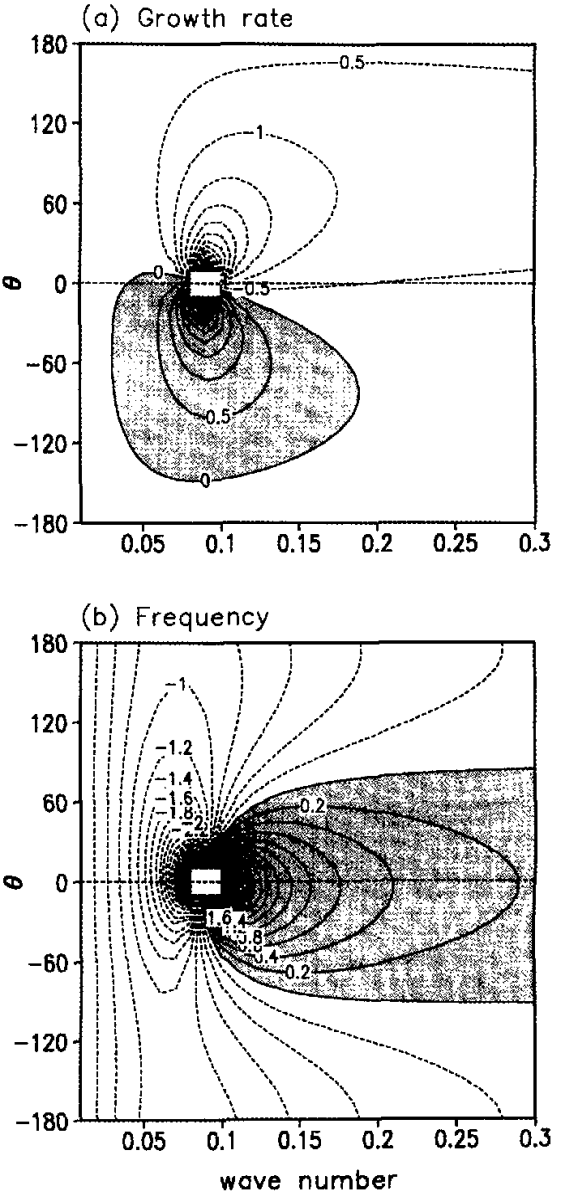

Fig. 1. (a) Growth rate and (b) frequency on the wave number and θ domain calculated from Equation (3). θ is the zonal phase difference between the wind stress and SST anomalies. Units are yr^{-1}. Positive values are shaded.

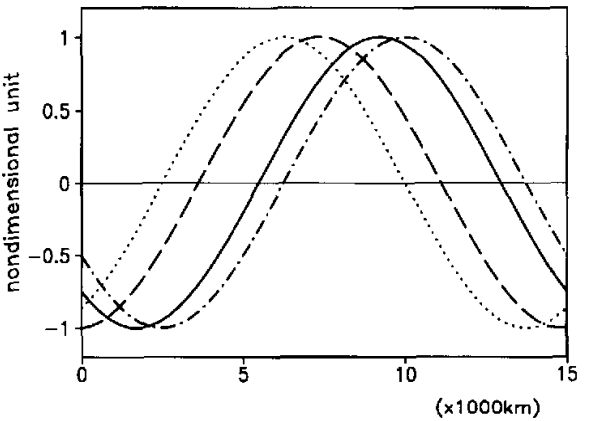

Fig. 2. Zonal structures of the SST (solid line), thermocline depth (dot–dashed line), wind stress (dotted line), and current (dashed line) anomalies associated with the fastest growing mode. Here x–axis corresponds to basin length. The nondimensional wave number of 0.15 is used.

obtained based on the equations of eigenvectors shown in the appendix. The quadrature relationship between the wind stress and thermocline depth still holds. Therefore, the warming by the thermocline effect appears far to the east of the SST (slightly to the west of cold SST), and the thermocline effect produces cooling in the warm SST region. Moreover, the zonal advection reinforces the cooling in the warm SST region. Therefore, the system damps and propagates to the east with a relatively fast speed. It is important to note that as demonstrated by Yamagata (1985), the wind stress and the zonal current are approximately in phase for the unstable mode (Fig. 3a), whereas the damped mode has an out of phase relationship between the two variables (Fig. 3b). It appears that the current for the unstable mode is mainly induced by the direct wind stress forcing, while that for the damped mode is balanced with the pressure gradient of thermocline depth.

For a further shift of wind stress to either west or east of SST, the present coupled system has the westward–propagating mode as indicated in Fig. 1b. In this case, the downwelling (upwelling) thermocline depth is located at the west of warm (cold) SST, and the thermocline effect enforces the coupled system to move to the west. As in the case of eastward propagating mode, the instability is closely related to the phase relationship between the current and wind stress anomalies. In other words, the unstable mode has the westerly (easterly) current located slightly west of the westerly (easterly) wind stress, and for the damped mode, the current and wind stress are almost out of phase.

4. Thermocline and zonal advection effects

In this section, two thermodynamic processes of thermocline and zonal advection effects in Eq. (2c) are separately examined. First, we consider the SST equation without the zonal advection ($\lambda=0$ and consequently $Y_1 = Y_2 = 0$), and therefore it is governed mainly by

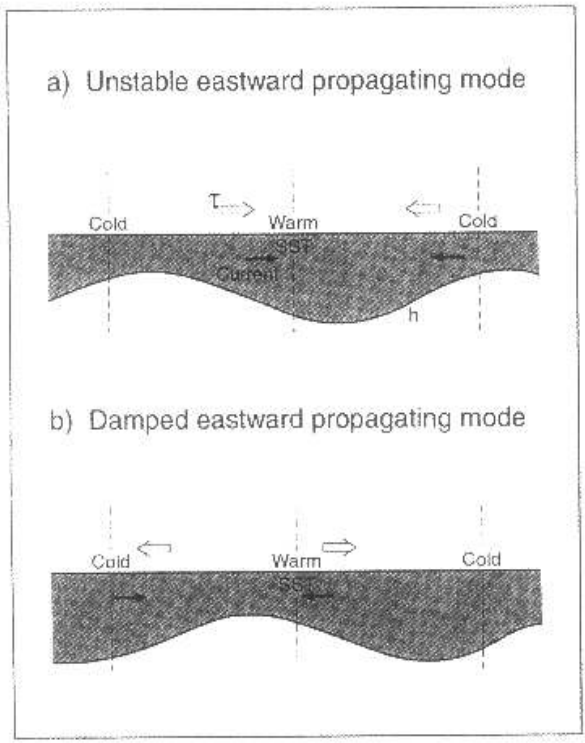

Fig. 3. Schematic diagram of wind stress (thick arrow), current (thin arrow), SST (indicated by "warm" and "cold"), SST tendency (the warm and cold SST tendencies are indicated by the solid and dashed line boundaries, respectively), and thermocline depth (contour) for (a) unstable and (b) damped eastward propagating modes.

the thermocline effect. In this case, the dispersion relationship can be simplified as

$$\omega_R = \frac{Y_3}{X_1}\cos\theta, \tag{4a}$$

$$\omega_I = \nabla - \frac{Y_3}{X_1}\sin\theta - \frac{X_2}{X_1}. \tag{4b}$$

Using the above equations, the growth rate and frequency are obtained in terms of wavenumber and the zonal phase difference (θ) between SST and wind stress and those are displayed in Figs. 4a and 4b. The figures indicate that the system is unstable for $-\pi<\theta<0$ and stable for $\pi>\theta>0$, and the system moves to the east for $|\theta|<\pi/2$ and to the west for $|\theta|>\pi/2$. This is because the quadrature relationship between the wind and thermocline depth holds in the present system. For $\theta=-\pi/2$, the SST warming region due to the thermocline change coincides with the region of warm SST, resulting in the maximum instability but no

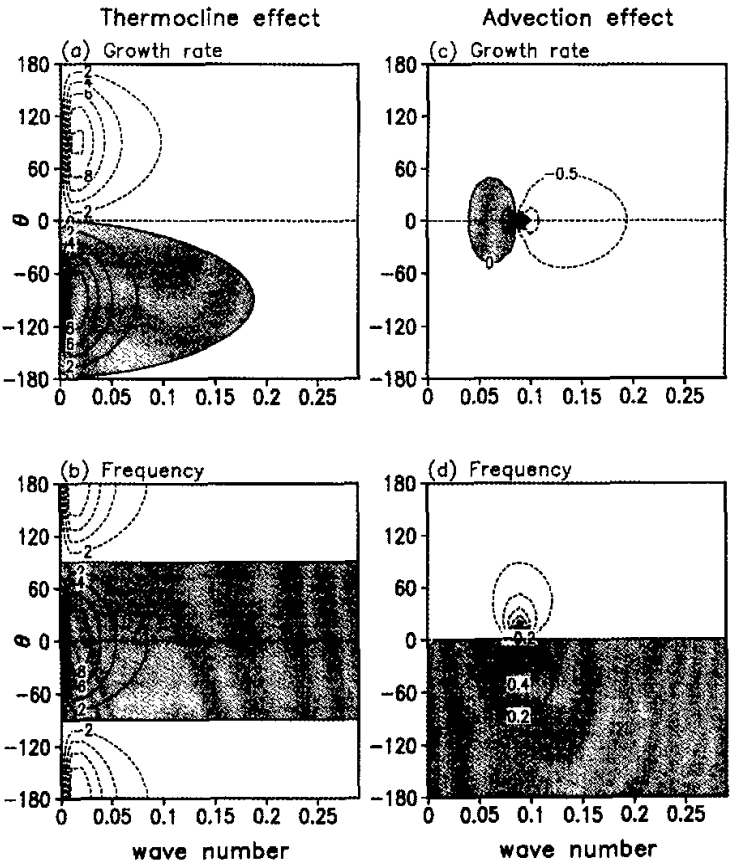

Fig. 4. As in Fig. 1 except for the thermocline effect alone case in (a) and (b), and the zonal advection effect alone case in (c) and (d).

propagation. On the other hand, the system has a maximum eastward phase speed for $\theta = 0$ because the maximum warm SST tendency appears at 90 degrees east of the warm SST. For $\theta = \pi$, the maximum warm SST tendency is located at 90 degrees west of the warm SST, resulting in the maximum westward propagation. It is also noted that the absolute values of the growth rate and frequency increase with the increase of wave scale, except for very long waves with the wavenumber k near zero. From the figures, the coupled system with the thermocline effect only can have unstable eastward propagating waves when large-scale winds are located west of SST with the phase difference less than $\pi / 2$.

For the case of zonal advection effect alone ($\sigma = 0$ and $Y_3 = 0$), the frequency and growth rate can be written as

$$\omega_R = \frac{(X_1 Y_2 - X_2 Y_1)\sin\theta}{X_1^2 + Y_1^2 - 2X_1 Y_1 \cos\theta}, \tag{5a}$$

$$\omega_I = \frac{(X_1 Y_2 + X_2 Y_1)\cos\theta - X_1 X_2 - Y_1 Y_2}{X_1^2 + Y_1^2 - 2X_1 Y_1 \cos\theta}. \tag{5b}$$

As shown in Fig. 4d, the moving direction of the coupled mode simply depends on the sign of θ. The system propagates to the east for $-\pi < \theta < 0$ and to the west for $\pi > \theta > 0$. This is because the wind and current anomalies are out of phase. This out of phase relationship is due to the balance between the current and the pressure gradient of the thermocline depth, and thus the SST tendency due to the zonal advection is out of phase with the wind stress. The large value of frequency occurs for a particular wavenumber near $k = 0.1$, where a singularity appears in the system with the two thermodynamic terms as shown in Fig. 1. Therefore, the singularity in Fig. 1 appears due to the zonal advection. Also note in Fig. 4c that the unstable mode appears for long waves of the wavenumbers between 0.05 and 0.1 and for the westerly (easterly) wind located near warm (cold) SST.

Comparison between the eigenmodes of the system with the thermocline effect only and those of advection effect only indicate that the thermocline effect plays a vital role in the propagation and instability of the coupled system. However, the zonal advection plays an important role for the wavenumbers near 0.1. It is also noted that the eigenmodes with both mechanisms shown in Fig. 1 differ from those with any of one mechanism. But, except for ultra-long waves, the characteristics of the eigenmodes shown in Fig. 1 mimic those of the eigenmodes with the thermocline effect only. The zonal advection modifies the eigenmodes in the ultra-long wave regime and produces the singularity near the wavenumber 0.1.

5. Summary

An eigen analysis of the equatorial air-sea coupled model is performed to understand the mechanism of the slowly varying mode for various zonal phase differences between SST and wind stress. The frequency and growth rate of the slow mode highly depend on the zonal phase between SST and wind stress anomalies. For the scale of the Pacific basin, the eastward propagating unstable modes appear when the westerly (easterly) wind stress is located to the west of the warm (cold) SST within a few thousand kilometer. These characteristics are consistent with the observed (Hirst, 1986).

The moving direction of the slow mode is closely related to the relative distance between the SST and wind stress anomalies. When the SST and wind stress anomalies are close to each other, the slow mode tends to propagate eastward. On the other hand, when the wind stress is located far away from SST, the slow mode tends to propagate westward. The instability of the coupled system depends on the net warming (cooling) tendency in the warm (cold) SST region. Because of the quadrature relationship between the wind stress and thermocline depth, the thermocline effect produces the unstable mode for the wind stress located 90 degrees west of the SST. On the other hand, the zonal advection produces the unstable mode for the wind stress near SST. The coupled system with both effects is unstable when the westerly (easterly) wind stress is located west of warm (cold) SST, and when the wind stress and SST are almost in phase, it becomes most unstable where the wave scale is about the Pacific basin scale. It is also noted that the system behavior highly depends on the wave scale. For the wave scales shorter than 20,000 km, the SST tendency in the present system is determined mainly

by the vertical advection due to the change of thermocline depth but modified by the zonal advection. However, the eigenmode characteristics of the ultra-long wave much longer than the Pacific basin scale are different from those with only one mechanism. Ultra-long waves propagate to the west regardless of the position of the wind stress.

Finally, it is noted that the wind stress and the zonal current are approximately in phase for the unstable mode, whereas the damped mode has an out-of-phase relationship between the two variables. These relationships for the unstable and damped modes are consistent with those demonstrated by Yamagata (1985). It appears that the current for the unstable mode is mainly balanced with the wind stress, while that of the damped mode is balanced mainly by the pressure gradient of thermocline depth.

Soon-Il An was supported by Frontier Research System for Global Change through its sponsorship of International Pacific Research Center, and In-Sik Kang was supported by the Brain Korea 21 Project and the SRC project of Korean Science and Technology Foundation. The authors thank Diane Henderson for her careful reading and editing of the manuscript. SOEST Contribution Number is 5285. IPRC contribution number is IPRC-63.

REFERENCES

An S.-I., and B. Wang, 2000: Interdecadal change of the structure of the ENSO mode and its impact on the ENSO frequency. *J. Climate*, **13**, 2044-2055.

Anderson D. L. T., and J. P. McCreary, 1985: Slowly propagating disturbances in a coupled ocean-atmosphere model. *J. Atmos. Sci.*, **42**, 615-629.

Battisti D. S., and A. C. Hirst, 1989: Interannual variability in the tropical atmosphere / ocean system: Influence of the basic state and ocean geometry. *J. Atmos. Sci.*, **46**, 1687-1712.

Cane M. A., and S. E. Zebiak, 1985: A theory for El Niño and the Southern Oscillation. *Science*, **228**, 1084-1087.

Dewitte B., and C. Perigaud, 1996: El Niño - La Niña events simulated with Cane and Zebiak's model and observed with satellite or ii situ data, Part II: model forced with observations. *J. Climate*, **9**, 1188-1207.

Hirst A. C., 1986: Unstable and damped equatorial modes in simple coupled ocean-atmosphere models. *J. Atmos. Sci.*, **43**, 606-630.

Hirst A. C, 1988: Slow instabilities in tropical ocean basin-global atmosphere models. *J. Atmos. Sci.*, **45**, 830-852.

Hoerling M. P., A. Kumar, and M. Zhong, 1997: El Niño, La Niña, and the nonlinearity of their teleconnections. *J. Climate*, **10**, 1769-1786.

Jin F.-F., 1997: An equatorial ocean recharge paradigm for ENSO. Part I: Conceptual model. *J. Atmos. Sci.*, **54**, 811-829.

Jin F.-F., and J. D. Neelin, 1993: Modes of interannual tropical ocean-atmosphere interaction - a unified view. Part I: Numerical results. *J. Atmos. Sci.*, **50**, 3477-3503.

Kang I.-S., and S.-I. An, 1998: Kelvin and Rossby wave contributions to the SST oscillation of ENSO. *J. Climate*, **11**, 2461-2469.

Kang I.-S., and J.-S. Kug, 2000: An El-Niño prediction system using an intermediate ocean and a statistical atmosphere. *Geophy. Res. Lett.*, **27**, 1167-1170.

Kirtman B. P., 1997: Oceanic Rossby wave dynamics and the ENSO period in a coupled model. *J. Climate*, **10**, 1690-1704.

Lau K. M., 1981: Oscillations in a simple equatorial climate system. *J. Atmos. Sci.*, **38**, 248-261.

Lau N. C., S. G. H. Philander, and M. J. Nath, 1992: Simulation of El Niño / Southern Oscillation phenomena with a low-resolution coupled general circulation model of the global ocean and atmosphere. *J. Climate*, **5**, 284-307.

Meehl G. A., 1990: Seasonal cycle forcing of El Niño-Southern Oscillation in a global coupled ocean-atmosphere GCM. *J. Climate*, **3**, 72-98.

Perigaud C., and B. Dewitte, 1996: El Niño-La Niña events simulated with Cane and Zebiak's model and observed with satellite or in situ data, Part I: model data comparison. *J. Climate*, **9**, 66-84.

Wakata, Y., and E. S. Sarachik, 1991: Unstable coupled atmosphere-ocean basin modes in the presence of a spatially varying basic state. *J. Atmos. Sci.*, **48**, 2060-2077.

Yamagata T., 1985: Stability of a simple air-sea coupled model in the tropics. Coupled Ocean-Atmosphere Models. *J. C. Nihoul, Ed., Elsevier Oceanography Series No.* **40**, 637-657.

Zebiak S. E., and M. A. Cane, 1987: A model El Niño-Southern Oscillation. *Mon. Wea. Rev.*, **115**, 2262-2278.

Appendix

The eigenvectors are

$$h(x,y,t)= I_c \exp(-(y/L_y)^2)e^{i(kx-\omega t)}, \tag{A1}$$

$$u(x,y,t)= I_c \frac{\omega+ia}{k}\exp(-(y/L_y)^2)e^{i(kx-\omega t)}, \tag{A2}$$

$$T(x,y,t)= I_c \frac{\lambda(\omega+ia)+k\sigma}{k(b-i\omega)}\exp(-(y/L_y)^2)e^{i(kx-\omega t)}, \tag{A3}$$

$$U(x,y,t)= I_c \frac{K_Q[\lambda(\omega+ia)+k\sigma]e^{-i\theta}}{(b-i\omega)(AB+k^2C^2)}\exp(-(y/L_y)^2)e^{i(kx-\omega t)}, \tag{A4}$$

$$\Theta(x,y,t)= I_c \frac{AK_Q[\lambda(\omega+ia)+k\sigma]e^{-i\theta}}{k(i\omega-b)(AB+k^2C^2)}\exp(-(y/L_y)^2)e^{i(kx-\omega t)}, \tag{A5}$$

where I_c and L_y are the amplitude constant and the meridional scale, respectively.